

Supplementary Material for

The commensal microbiome is associated with anti–PD-1 efficacy in metastatic melanoma patients

Vyara Matson, Jessica Fessler, Riyue Bao, Tara Chongsuwat, Yuanyuan Zha,
Maria-Luisa Alegre, Jason J. Luke, Thomas F. Gajewski*

*Corresponding author. Email: tgajewsk@medicine.bsd.uchicago.edu

Published 5 January 2018, *Science* **359**, 104 (2017)
DOI: 10.1126/science.aaq3290

This PDF file includes:

Materials and Methods

Figs. S1 to S9

References

Other Supplementary Material for this manuscript includes the following:
(available at www.sciencemag.org/content/359/6371/104/suppl/DC1)

Tables S1 to S6 as separate Excel file

Materials and Methods

Patient fecal sample collection

Stool samples were collected from 42 metastatic melanoma patients prior to immunotherapy initiation. Eligible patients were provided an EasySampler Collection Kit (ALPCO) to collect stool sample at home. The stool samples were brought to the lab within 24 hours after collection. DNA was immediately isolated from 250 mg of stool and the rest of the sample was aliquoted and stored at -80°C. .

Microbial DNA isolation

Patient stool samples were handled under BSL2 laminar flow hood using sterile technique. The technician wore gloves, gown, face mask and hair net to prevent contamination of the samples. Isolation of microbial DNA from patient and mouse fecal samples was performed using QIAamp PowerFecal DNA Kit and QIAamp DNA Stool Mini Kit, respectively (Qiagen, Germantown, MD), including a bead-beating step. DNA concentration was measured using a Nanodrop-nd1000 and the DNA was stored at -80°C.

16S rRNA gene amplicon library preparation and sequencing

16S rRNA gene amplicon library preparation and sequencing was performed at the Argonne National Laboratory. Briefly, PCR amplicon libraries targeting the 16S rRNA encoding gene were produced using a barcoded primer set adapted for the Illumina HiSeq2000 and MiSeq (17). DNA sequence data were then generated using Illumina paired-end sequencing at

the Environmental Sample Preparation and Sequencing Facility (ESPSF) at Argonne National Laboratory. Specifically, the V4 region of the 16S rRNA gene (515F-806R) was PCR-amplified with region-specific primers that include sequencer adapter sequences used in the Illumina flowcell (17, 18). The forward amplification primer also contains a twelve-base barcode sequence that supports pooling of up to 2,167 different samples in each lane (17, 18). Each 25 µL PCR reaction contained 9.5 µL of MO BIO PCR Water (Certified DNA-Free), 12.5 µL of QuantaBio's AccuStart II PCR ToughMix (2x concentration, 1x final), 1 µL Golay barcode tagged Forward Primer (5 µM concentration, 200 pM final), 1 µL Reverse Primer (5 µM concentration, 200 pM final), and 1 µL of template DNA. The conditions for PCR were as follows: 94 °C for 3 minutes to denature the DNA, with 35 cycles at 94 °C for 45 s, 50 °C for 60 s, and 72 °C for 90 s; with a final extension of 10 min at 72 °C to ensure complete amplification. Amplicons were then quantified using PicoGreen (Invitrogen) and a plate reader (Infinite® 200 PRO, Tecan). Once quantified, volumes of each of the products were pooled into a single tube so that each amplicon was represented in equimolar amounts. This pool was then cleaned up using AMPure XP Beads (Beckman Coulter) and quantified using a fluorometer (Qubit, Invitrogen). The pool was diluted down to 2 nM, denatured, and further diluted to a final concentration of 6.75 pM with a 10% PhiX spike for sequencing on the Illumina MiSeq. Amplicons were sequenced on a 151bp x 12bp x 151bp MiSeq run using previously described sequencing primers and procedures (17). The average sequencing depth for the patient samples was 51,029, ranging from 28,040 to 68,928 reads; the average sequencing depth for mouse samples was 158,728, ranging from 54,632 to 327,216 reads per sample.

Microbial 16S rRNA gene amplicon analysis

The microbial 16S rRNA gene amplicon sequencing data from human and mouse fecal collections were processed separately with Quantitative Insights Into Microbial Ecology (QIIME) (version 1.91) (19) using similar protocols as previously described (4). In brief, raw reads were trimmed to remove low quality bases and paired-end 3' overlapping mates were merged using SeqPrep (<https://github.com/jstjohn/SeqPrep>). The open reference OTU picking protocol was used at 97% sequence identity against the Greengenes database (08/2013 release) (20). PyNAST was used to align sequences (21) and uclust consensus taxonomy assigner was used for taxonomic assignment (22). Data were rarefied to an even depth of 13,190 reads for the human microbial cohort and 22,560 reads for the mouse microbial cohort, respectively. OTUs occurring in less than 10% of the samples were removed per comparison in each cohort. Permutation tests (also known as, non-parametric *t*-tests in QIIME v1.9 manual) using Monte Carlo simulation were performed to identify differences in bacterial taxa occurrence between fecal communities of responders (R) and non-responders (NR) from human samples, and between slow and fast tumor growth groups from human microbiota-colonized mice. The tools and parameters used in each analysis step are described as follows:

- 1) The FastQ files were demultiplexed based on unique sample barcodes using *split_libraries_fastq.py* and paired-end reads were merged based on overlapping 3' end mates using *join_paired_ends.py* (SeqPrep method with low quality base trimming and adaptor clipping turned on by default).
- 2) Reads were clustered into OTUs based on 97% sequence similarity and searched against reference database followed by de novo assembly of clustered sequences using *pick_open_reference_otus.py*, with option “enable_rev_strand_match” set to TRUE and requiring at least 2 sequences per OTU for singleton removal. The OTU abundance

table was generated and phylogenetic tree was reconstructed. 3) All samples were rarefied to the same sequencing depth using *single_rarefaction.py* based on the least number of reads mapped per sample. 4) Alpha (e.g. Shannon index) and beta diversity metrics were collected using *core_diversity_analyses.py*, and compared between NR and R groups using *compare_alpha_diversity.py* (option “nonparametric” test with Monte Carlo permutations) and *compare_categories.py* (ANOSIM and PERMANOVA methods with weighted UniFrac distance), respectively, with 999 permutations and FDR correction for multiple comparisons. 5) OTUs were filtered for those present in at least 10% of the samples using *filter_otus_from_otu_table.py*, leaving 2,181 OTUs in the human 16S dataset and 3,235 OTUs in the mouse 16S dataset for statistical comparison of group differences. 6) OTUs differentially abundant between NR and R groups were identified by permutation test implemented in *group_significance.py* with option “nonparametric_t_test” and 1000 permutations, and filtered by a statistical significance level of 0.05 for subsequent analysis.

Analysis of the mouse 16S dataset revealed 519 OTUs differentially abundant between the fast and slow tumor growth groups at FDR-adjusted $P < 0.05$. Among these, 298 OTUs were assigned with known reference IDs and 221 with new reference ID. The new reference OTU IDs are not comparable between different cohorts, hence we focused on the OTUs with known reference IDs. Out of 298 OTUs, 207 OTUs were matched with human donors and used for generation of the heatmap depicted in Figure 3B. In addition, binary Bray–Curtis dissimilarity index was computed for each donor-mouse sample pair based on presence/absence of matched OTUs. For each pair, OTUs of relative abundance > 0.0001 in the donor or the mouse sample was included for the calculation.

BLASTN methodology

To investigate the identity of the OTUs differentially abundant between responders and non-responder patients, the assembled 16S rRNA gene amplicon sequences were characterized by a BLAST search against NCBI bacterial nucleotide sequence database (the search results were last updated on 10/04/2017). Using the blastn command line tool and the “megablast” program selection method, the top hits with ≥98% identity to the query sequence were returned from the nucleotide collection database restricted to bacteria, and excluding environmental or uncultured sample sequences. Results are shown in table S3. For some OTUs there were no hits with ≥98% identity and the top 10 hits are listed regardless of the percent identity value.

Metagenomic shotgun sequencing

Metagenomic shotgun sequencing was performed at the Marine Biological Laboratory affiliated with the University of Chicago. Briefly, the quantity of the DNA sample was measured using Picogreen (Invitrogen). DNA was then sheared using a Covaris and the libraries were constructed with the Nugen Ovation Rapid DR Multiplex System (PCR-free). The aimed insert size is between 400-600 bp. Amplified libraries were visualized on an Agilent DNA1000 chip or Caliper HiSens Bioanalyzer assay, pooled at equimolar concentrations and size selected using a Sage PippinPrep 2% cassette. The library pool was quantified using a Kapa Biosystems qPCR library quantification protocol, then sequenced on the Illumina NextSeq in a 2x150 paired-end sequencing run using dedicated read indexing. The samples were demultiplexed with bcl2fastq. An average of 80.4 million reads were generated per sample, ranging from 38.9 to 156.7 million

reads.

Microbial shotgun metagenomics analysis

The microbial shotgun metagenome sequencing data from human fecal collections were taxonomically profiled using Metagenomic Phylogenetic Analysis (MetaPhlAn 2) (23). Species-level taxonomic relative abundances were inferred for all samples following protocols detailed elsewhere (24). In brief, host contamination in the metagenomic reads was identified using KneadData version 0.61 (<http://huttenhower.sph.harvard.edu/kneaddata>) with human (GRCh37) reference databases (example command: kneaddata -i fq1 -i fq2 -db kneaddataDB -o out --output-prefix sample -t threads -q phred33 --trimmomatic trimmomaticPath --max-memory 2048m --trimmomatic-options 'LEADING:20 TRAILING:20 AVGQUAL:30 SLIDINGWINDOW:4:20 MINLEN:70 TOPHRED33' --run-trf). The high-quality reads were then mapped against a catalog of ~1 million clade-specific marker sequences identified from ~17,000 reference genomes currently spanning bacteria, archaea, eukaryotes and virus phylogenies to assign reads to microbial clades (example command: metaphlan2.py in1,in2 --bowtie2out out.bowtie2.bz2 --nproc threads --input_type fastq > out.txt). The relative abundance of each taxonomic unit in each sample was estimated by normalizing read counts assigned to each clade by the nucleotide length of its markers and by the sum of all weighted read counts in this clade including all subclades (example command: metaphlan2.py out.bowtie2.bz2 --nproc threads --input_type bowtie2out -t rel_ab > out.rel_ab.txt). To compare species identified from 16S and shotgun sequencing, the profiled bacterial species were then compared to the taxonomy of OTUs generated from 16S sequencing at family level, and the statistical

dependence between the relative abundance of 16S OTUs and each matched shotgun species was determined using Spearman's rank correlation tests, followed by filtering for those with positive correlation and at $P < 0.05$.

qPCR validation of metagenomic and 16S rRNA gene sequencing of fecal samples

The abundance of some of the bacterial species identified with the metagenomic and 16S rRNA gene amplicon sequencing approaches were further measured by qPCR using previously validated subgroup- or species-specific primers and probes (25-37) and SYBR Green or TaqMan PCR master mix (Applied Biosystems). The primers and probes were synthesized by Integrated DNA Technologies (Coralville, IA) and Life Technologies, respectively. qPCR was performed on StepOnePlus Real-Time PCR System (Applied Biosystems, Foster City, CA) and analyzed with StepOnePlus Software. The primer concentrations were as previously described (Table S5). The cycling conditions for the TaqMan-based reactions were 50°C for 2 min, 95°C for 10 min, 40 cycles of 95° for 15 secs, 60-65°C for 1 min, with varying annealing temperatures depending on the primer pair. The cycling conditions for the SYBR Green-based reactions were 95°C for 10 min, 40 cycles of 95° for 15 sec, 60-75°C for 10-40 sec, 72°C for 20-50 sec, with varying annealing temperatures and times depending on the primer pair. Fluorescence signal was detected at the end of each cycling stage. For some reactions, fluorescence detection was done during an additional 15 sec step at a higher temperature to minimize signal from primer dimers and minor non-target products (26). Melt curve analysis was performed to confirm amplification specificity. The results were expressed as relative abundance normalized to the total bacterial load. Specifically, to calculate the total bacterial load, qPCR was performed using

previously described universal bacterial primers (38). A standard curve was generated using the PCR blunt vector (Invitrogen) containing a single copy of the 16S rRNA gene derived from a member of the *Porphyromonadaceae* family (39) and the total 16S rRNA gene copies per ng DNA was calculated for each sample. Relative abundance for each species was expressed as 2^{-Ct} normalized to the number of total 16S rRNA gene copies per ng DNA in each sample and multiplied by a constant (7.3×10^{19}) to bring all values larger than 1. A summation qPCR score was computed per individual sample taking into consideration the abundance of 10 validated qPCR targets (*Enterococcus faecium*, *Collinsella aerofaciens*, *Bifidobacterium adolescentis*, *Klebsiella pneumoniae*, *Veillonella* sp., *Parabacteroides merdae*, *Lactobacillus* sp., *Bifidobacterium longum*, *Ruminococcus obeum* and *Roseburia intestinalis*). First, data transformation was applied on the relative abundance to bring signal close to Gaussian distribution. The relative abundance of each species was log10 transformed, and scaled by dividing the value by their root mean square across samples. The abundance of *Ruminococcus obeum* and *Roseburia intestinalis* (more abundant in non-responders) were multiplied by (-1). The sum of the transformed abundance of the 10 qPCR results was calculated to generate the score, and compared between groups of interest using two-sided Student's *t*-test.

RNAseq of tumor samples and data analysis

RNA was isolated from tumor samples using the QIAGEN AllPrep DNA/RNA FFPE kit (Qiagen, Hilden, Germany) according to the manufacturer's instructions. The quality of RNA was measured on Agilent 2100 Bioanalyzer (Agilent Technologies, Santa Clara, USA). cDNA was reverse transcribed from RNA and used for library preparation following dUTP strand-specific

protocol by the University of Chicago Genomics Core Facility. Ribosome RNA was removed using the Ribo-Zero rRNA Removal Kit (Human) (Illumina, San Diego, USA). Sequence reads were generated on an Illumina HiSeq 4000 instrument at the Functional Genomics Facility. An average of 133.3 million 2x100bp paired-end (PE) reads were generated for each sample, ranging from 93.2 to 208.0 million reads. The quality of raw reads was assessed by FastQC (40) (v0.11.5). Reads were aligned to human reference transcriptome with Gencode gene annotation (v26, GRCh38) by Kallisto (41) (v0.43.1) with the strand-specific mode, which implements kmer-based pseudoalignment algorithm for accurate quantification of transcripts from RNAseq data and is robust to errors in the reads. Transcript abundance was quantified at transcript level specifying strand-specific protocol, summarized into gene level using tximport (42) (v1.4.0), normalized by trimmed mean of M values (TMM) method, and log2-transformed for further analysis. Selected transcripts (PD-L1 and PD-1) were compared between responders and non-responders.

Whole exome + UTR sequencing of tumor samples and data analysis

Tumor DNA was isolated from tumor samples using the QIAGEN AllPrep DNA/RNA FFPE kit (Qiagen, Hilden, Germany), and DNA integrity and quantification were evaluated on an Agilent 2100 Bioanalyzer (Agilent Technologies, Santa Clara, USA) and qubit (Thermo Fisher, Waltham, USA), respectively. Two hundred ng of DNA was used for whole exome + UTR capture using the Agilent SureSelect Human All Exon V6 plus UTR kit (Agilent Technologies, Santa Clara, USA). Sequence reads were generated on an Illumina NextSeq 500 instrument (Illumina, San Diego, USA) at the University of Chicago Functional Genomics Facility. An

average of 62.2 million 2x100bp paired-end (PE) reads were generated for each sample, ranging from 51.9 to 70.9 million reads.

The raw sequencing data were analyzed by an in-house pipeline constructed for WES analyses of paired or unpaired cancer genomes. The quality of raw reads is assessed by FastQC (40) (v0.11.5), and preprocessed to trim adaptors and merge 3' overlapping mates using SeqPrep (v1.2). Reads were aligned to human reference genome (GRCh37) using BWA-MEM (43) (v0.7.15) with soft-clipping option activated by default. Read duplicates were marked using Sambamba (44) (v0.6.3) and alignments of mapping quality<30 were removed. Reads alignment was further refined using insertions/deletions realignment and base quality score recalibration (BQSR) using GATK (45) (v3.8.0). Callable loci were collected from the alignment using GATK CallableLoci program, and merged with Agilent V6 + UTR exome capture target regions provided by the vendor. Since matched normal tissue was not available for sequencing, we detected putative somatic mutations by MuTect2 (46) (v3.8.0), which identifies somatic single nucleotide variants (SNVs) and indels from high-quality bases using the tumor-only mode. Stringent filters were applied on variants that passed the default setting of the caller to further remove potential germline variants identified as those present in dbSNP database, or at allele frequency (AF) \geq 0.0001 in 1000 Genomes Project (G1000) (47), the NHLBI Grand Opportunity Exome Sequencing Project (ESP) (48), or the Exome Aggregation Consortium (ExAC) (49) on non-TCGA samples. Variants that passed all filters were carried on for annotation using ANNOVAR (50) (June 2017 release). The somatic mutation burden was calculated by the total number of mutations that were predict to cause protein sequencing change, including non-

synonymous, stopgain, and stoploss SNVs, frameshift and non-frameshift indels, and variants that modify splicing sites.

Immunohistochemistry of tumor samples

Tissue sections were prepared from paraffin-embedded tumor samples from 5 responders and 10 non-responder patients. The slides were stained using Leica Bond RX automatic stainer. Bond™ Epitope Retrieval Solution I (Leica Biosystems, CatNo: AR9961) was applied for 20 minutes. A primary anti-CD8 antibody (clone C8/144B from Dako; 1:400 dilution) was applied for 25 minutes. The primary antibody was then detected with Bond™ Polymer Refine Detection kit (Leica Biosystems, CatNo: DS9800). The CD8⁺ cell density was expressed as a ratio of CD8⁺ cells/pixel to total cells/pixel using inForm® Cell Analysis™ software (PerkinElmer).

Animals, fecal transfer, and tumor model

Specific pathogen-free (SPF) C57BL/6 mice were obtained from Taconic Biosciences (Hudson, NY). SPF mice were fed Teklad irradiated 2918 diet (Envigo), or in some cases autoclaved 5K67 diet (Lab Diet, St. Louis, MO), and housed in the University of Chicago SPF animal facility. Germ-free (GF) C57BL/6 mice were initially purchased from Taconic biosciences, then bred and housed in flexible-film isolators in the University of Chicago Gnotobiotic Research Animal Facility and fed autoclaved 5K67 diet. Some GF mice were gifted by Dr. Eugene Chang at the University of Chicago. For all experiments, 6–8-week-old mice were used. The C57BL/6-derived melanoma cell line B16.F10.SIY (henceforth referred to as B16.SIY) was generated as described (51). For tumor growth experiments, some GF mice were colonized with fecal microbiota from 3 responders and 3 non-responder patients, or microbiota from SPF

mice by oral gavage. Briefly, 200 mg of human stool was thawed and suspended in 3 ml of PBS or mouse fecal pellets were collected fresh and suspended in 1 ml of PBS per pellet. After settling of the particulate material, each mouse was gavaged with 10 ml/kg body weight (approximately 200 µl per mouse) of the fecal supernatant. Two weeks after gavage, the colonized mice were injected subcutaneously with 1×10^6 B16.SIY tumor cells. Some mice were injected i.p. 7, 10, 13, and 16 days after tumor inoculation with 100 µg of anti-PD-L1 monoclonal antibody (BioXCell, 10F.9G2). Tumor size was measured three times per week until the endpoint and tumor volume was determined as length x width² x 0.5. Microbiota composition of the colonized mice was assessed with 16S rRNA gene amplicon sequencing of DNA extracted from fecal samples collected 4 weeks after colonization. Taconic SPF mice were used as a control. The experimental animal procedures were approved by the University of Chicago Animal Care and Use Committee.

SIY Pentamer analyses

For immune profiling, cells were labeled with a PE-MHC class I pentamer (Proimmune) consisting of murine H-2K^b complexed to SIYRYYGL (SIY) peptide or to an irrelevant SIINFEKL peptide. Tumor cell suspensions were subsequently stained with CD3-AlexaFluor700 (Ebioscience, 17A2), CD8α-Pacific Blue (Biolegend, 53-6.7), CD4-BrilliantViolet711 (Biolegend, RM4-5), CD44-FITC (BD, IM7), FOXP3-APC (Ebioscience, FJK-16a) and Fixable Viability Dye-eFluor780 (Ebioscience). The cells were then washed and fixed in 1% paraformaldehyde and analyzed on LSRFortessa flow cytometer with FACSDiva software (BD). Data analysis was performed using FlowJo software (Tree Star).

IFN- γ ELISPOT

ELISPOT was carried out using anti-IFN- γ capture/detection antibody pair from BD Biosciences. ELISPOT plates (Millipore, MAIP S4510) were coated with capture antibody (CatNo: 51-2525KD) overnight at 4°C and then blocked with DMEM + 10% FBS for 2 hours at room temperature. Splenocytes were enumerated using flow cytometry, plated at 10⁶ cells per well and stimulated with 160 nM SIY peptide or irrelevant OVA peptide as negative control, or 500 ng/ml ionomycin + 50 ng/ml PMA as positive control, overnight at 37°C. The following day, IFN- γ spots were detected with biotinylated detection antibody (CatNo: 51-1818KZ), followed by streptavidin-HRP and AEC substrate kit (all from BD Biosciences). The spot number and size were quantified using an Immunospot Series 3 Analyzer and ImmunoSpot software (Cellular Technology).

Statistical analysis

Tumor growth curves were analyzed using two-way ANOVA with Tukey's multiple comparisons post-test using GraphPad PRISM. For other comparisons between two groups, including evaluating significance in immune profiling or quantitative PCRs, unpaired, two-tailed Student's *t*-test or Wilcoxon-Mann-Whitney test (non-parametric) was used as indicated in the figure legends. Microbial composition comparisons were performed using permutation tests implemented in QIIME (option "nonparametric_t_test"). For multiple comparisons, p-value was adjusted using Benjamini-Hochberg FDR correction (52). Spearman's rank correlation coefficient ρ was used for measuring statistical dependence between relative abundance of bacteria produced by different platforms. $P<0.05$ was considered statistically significant and

denoted as follows: * $P < 0.05$, ** $P < 0.01$, *** $P < 0.001$, **** $P < 0.0001$. Statistical analysis was performed using GraphPad PRISM and R.

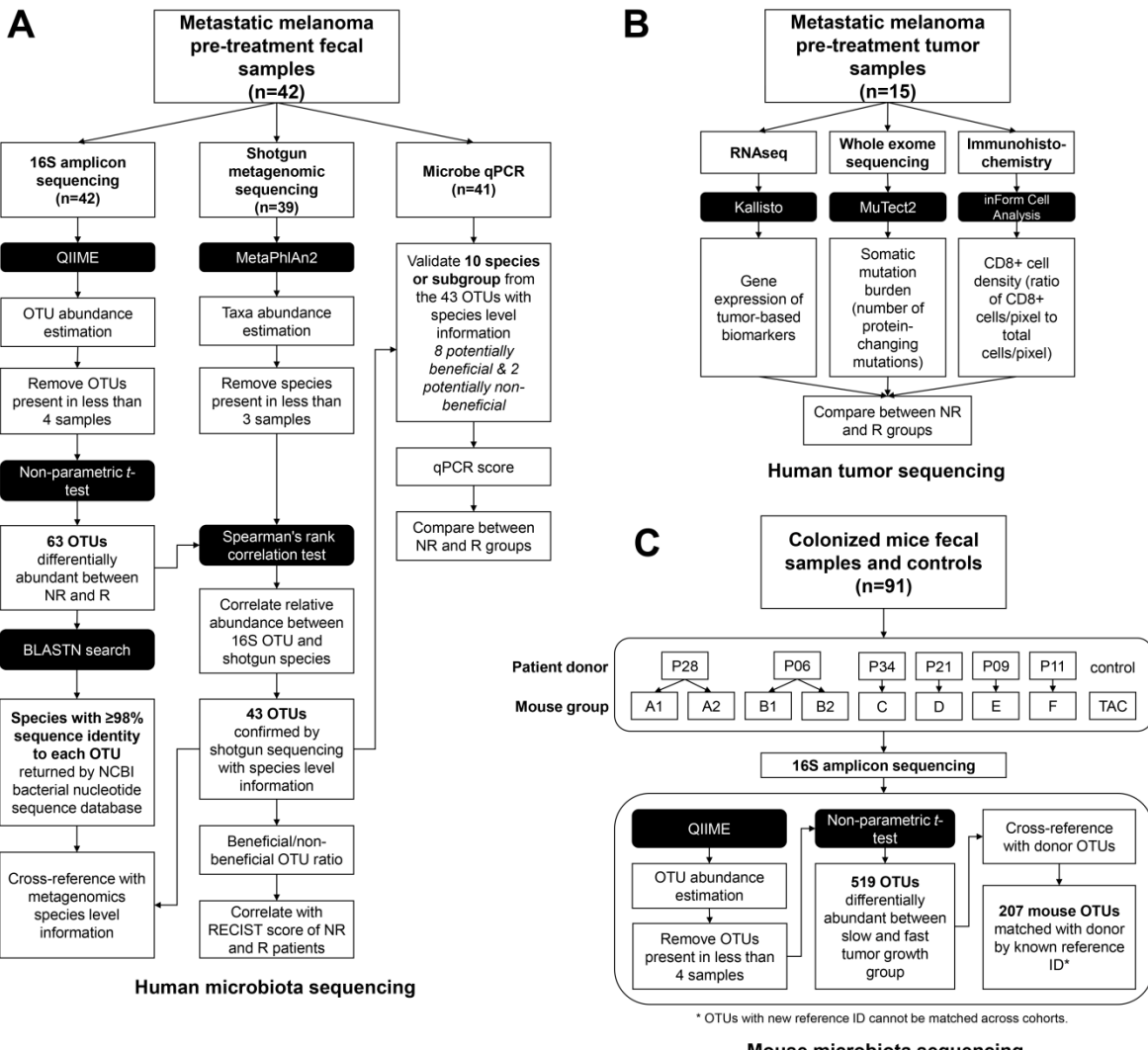


Fig. S1. Workflow schematic indicating (A) the integration of methods for microbial identification, (B) analyses of tumor-associated biomarkers, and (C) 16S sequencing-based identification of bacteria in patient stool samples with a potential role in modulating anti-tumor immunity in a mouse melanoma model.

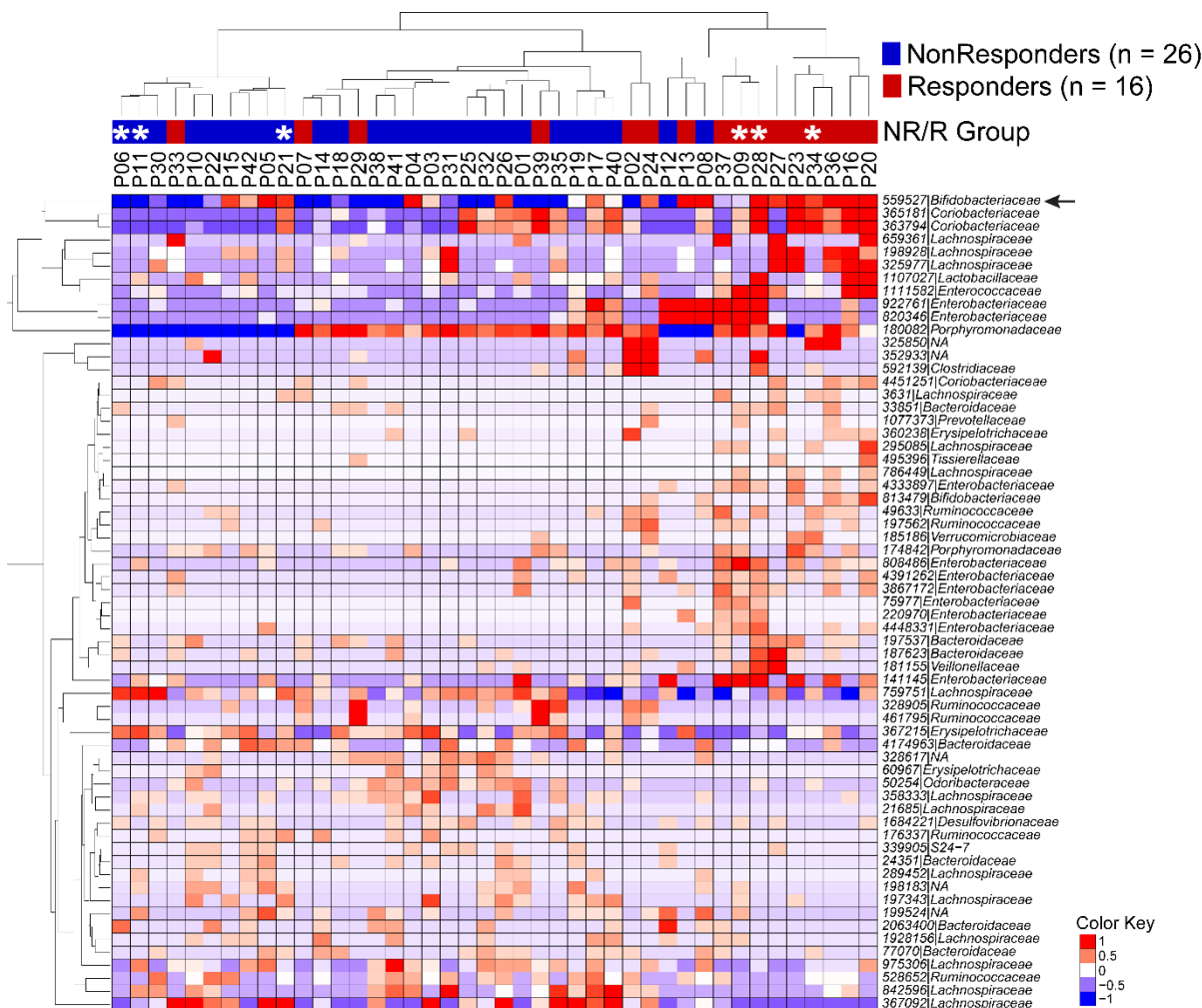


Fig. S2. Segregation of responder and non-responder samples based on relative abundance

data for the 63 differentially abundant OTUs determined with 16S sequencing using unadjusted, non-parametric *t* test. (62 OTUs were significantly different with P<0.05; 1 OTU, *Bifidobacteriaceae* OTU 559527 indicated with arrow, approached significance with P<0.058). Columns depict individual patients clustered using unsupervised hierarchical clustering with Euclidean distance. Asterisks indicate samples used in further in-vivo experiments. Annotation bar above the heatmap indicates clinical response to immunotherapy. The ID of *de-novo*

assembled OTUs (new clean-up reference OTUs picked by QIIME) were abbreviated to show only the unique identifier digits, and the full OTU IDs are provided in table S4.

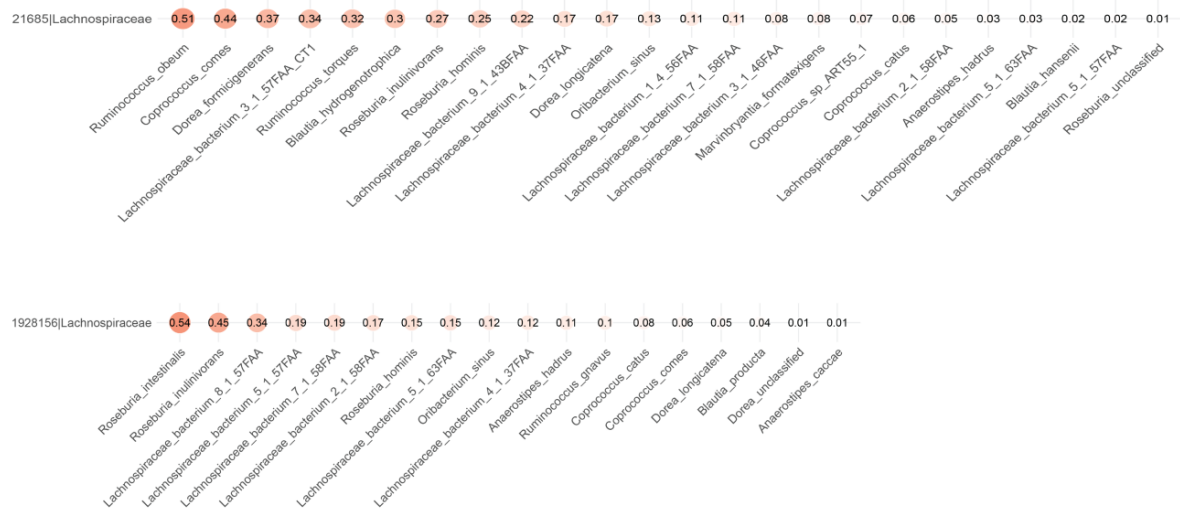
A**B**

Fig. S3. Ranked species-level identities of 16S OTUs predicted with shotgun sequencing. OTUs picked by 16S sequencing analysis were first matched to species identified by shotgun sequencing at the family level. Then, pairwise tie-corrected Spearman's correlation was computed for each matching pair and the species matched to each OTU were ranked based on the correlation coefficient ρ value. A complete list of the 63 OTU-to-species matching between the 16S and shotgun sequencing datasets is included in table S4.

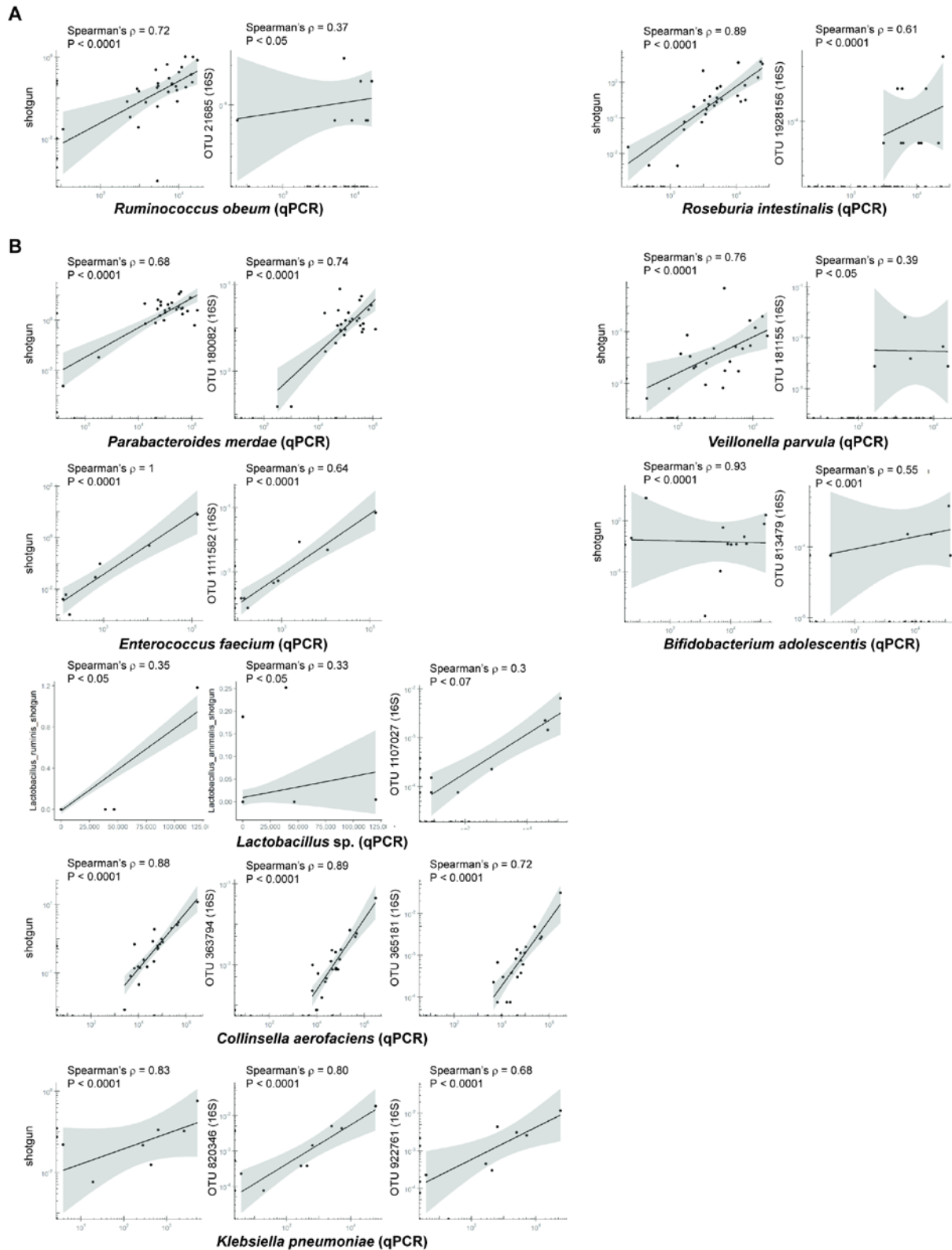


Fig. S4. Use of species-specific qPCR for additional confirmation of the OTU-to-species matches determined by 16S and shotgun sequencing data comparisons. OTUs and their best-match species as measured with 16S and shotgun sequencing, respectively, were correlated by Spearman's test against the relative abundance of the corresponding species measured with qPCR. Depicted are correlations for OTUs (and their best-match species), which are more abundant in non-responders (A) or in responders (B) and are used for computation of the qPCR score. Of note, OTU 1107027 (identified as *Lactobacillus ruminis* with 16S sequencing analysis) was best matched to *Lactobacillus animalis* (from the shogun sequencing data set) with $P<0.1$ (table S4) and was included in the qPCR score, because a primer set with a broader *Lactobacillus* sp. specificity was used (table S5).

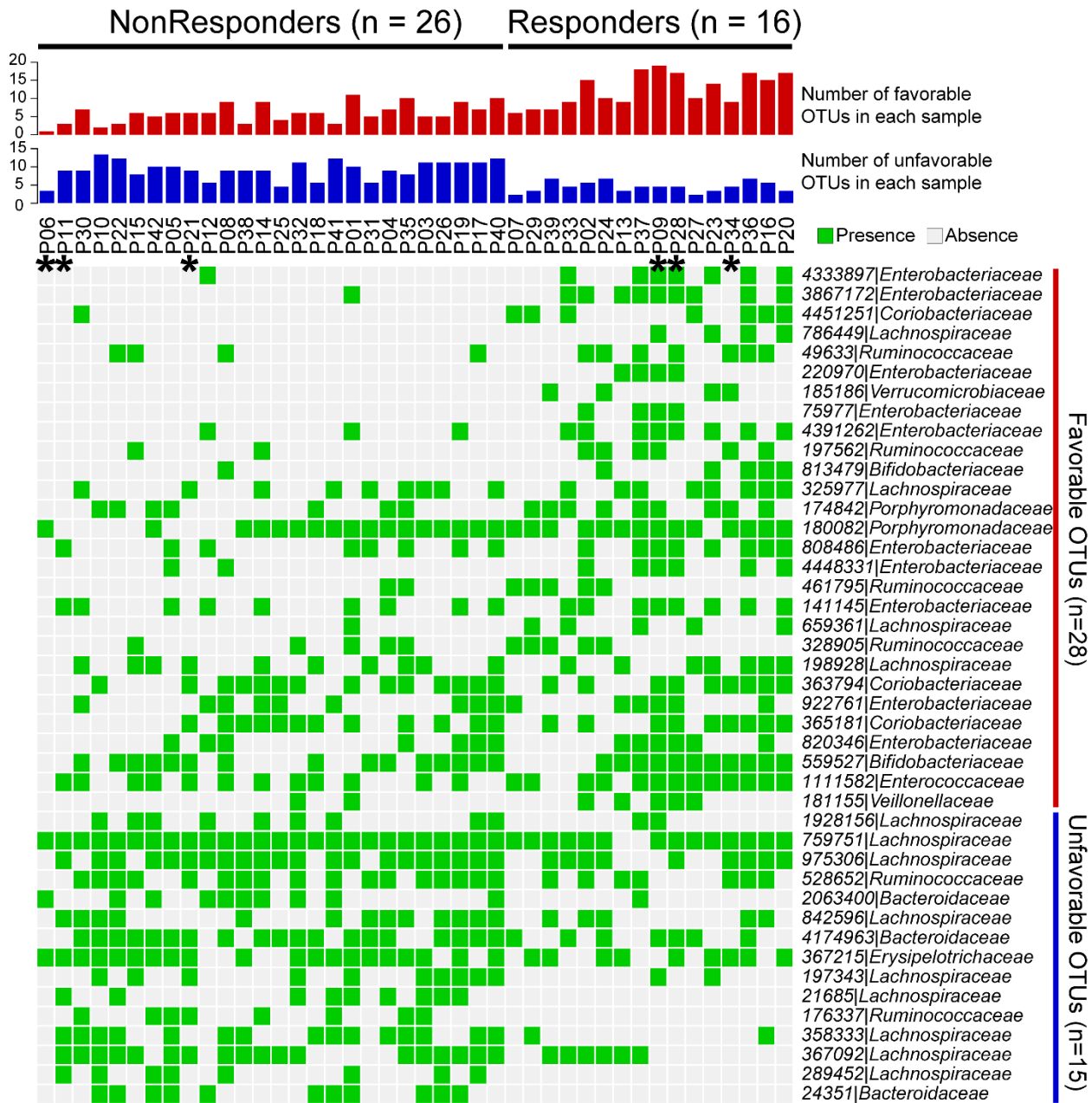


Fig. S5. Visual representation of the presence/absence-based ratio of beneficial/non-beneficial OTUs. The bar graphs represent the total number of potentially beneficial OTUs (more abundant in responders; depicted in red) and potentially non-beneficial OTUs (more

abundant in non-responders; depicted in blue) in each patient. The grid map represents presence (green) or absence (white) of beneficial and non-beneficial OTUs in each patient sample. Columns depict individual patients grouped based on clinical response to immunotherapy in the same order as in Figure 1A. Rows indicate the 43 OTUs from 16S sequencing that were confirmed by shotgun sequencing (table S4). Asterisks indicate samples used in further in-vivo experiments. The ID of *de novo* assembled OTUs (new clean-up reference OTUs picked by QIIME) were abbreviated to show only the unique identifier digits, and the full OTU IDs are provided in table S4.

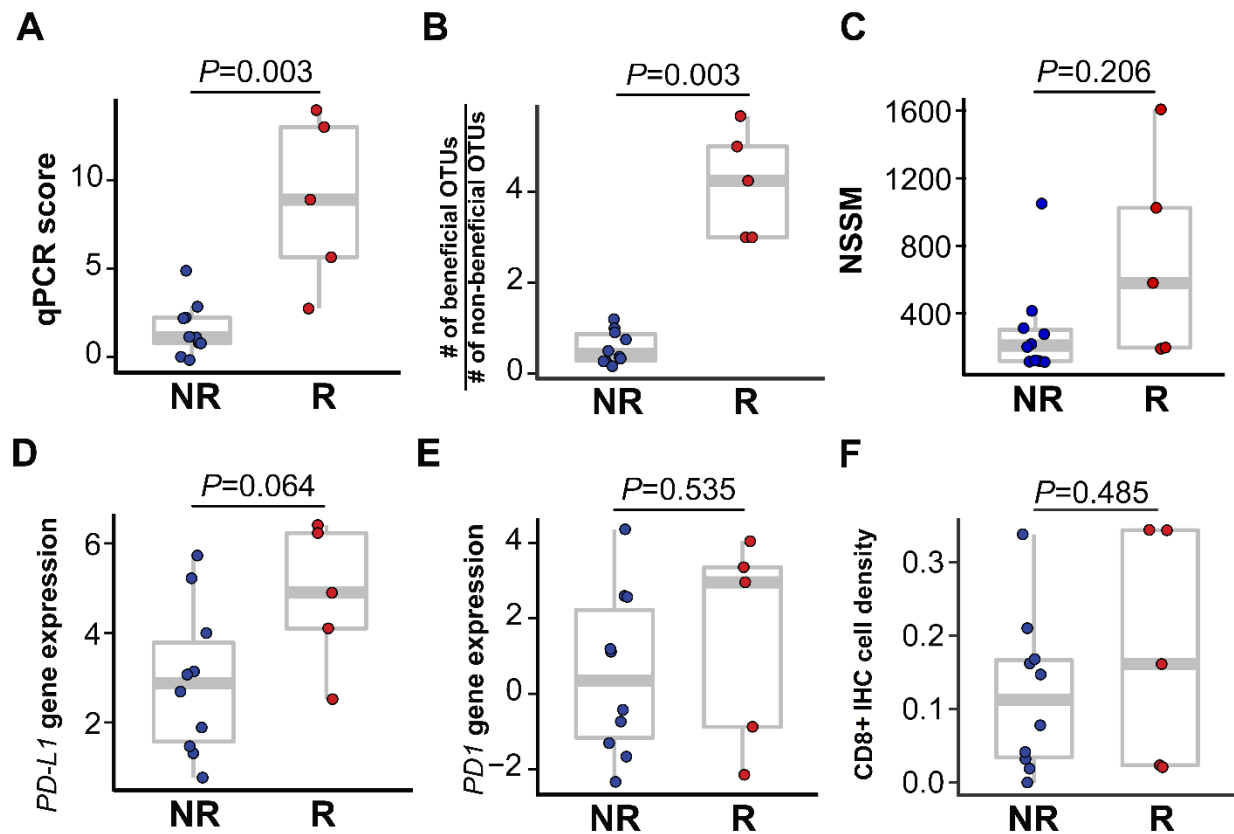


Fig. S6. The qPCR score and the beneficial/non-beneficial OTU ratio as candidate predictors of clinical response to immunotherapy. The qPCR score (**A**) and the ratio of beneficial-to-non-beneficial OTUs (**B**) were more distinct between non-responders (NR) and responders (R), compared to the non-synonymous somatic mutational (NSSM) load (**C**), expression levels of *PD-L1* (**D**) and *PD-1* (**E**), as determined by whole transcriptome sequencing of tumor samples, and intra-tumoral CD8⁺ T cell infiltration (**F**) as determined with immunohistochemistry of tumor samples. This analysis was limited to subset of 5 responders and 10 non-responders from the original 42 patient cohort, whose samples passed quality control for RNA sequencing. Wilcoxon-Mann-Whitney test (non-parametric) was used for comparing qPCR score, OTU ratio,

and NSSM between NR and R groups, which does not assume data follow normal distribution.

Student's *t*-test was used for the rest of the markers.

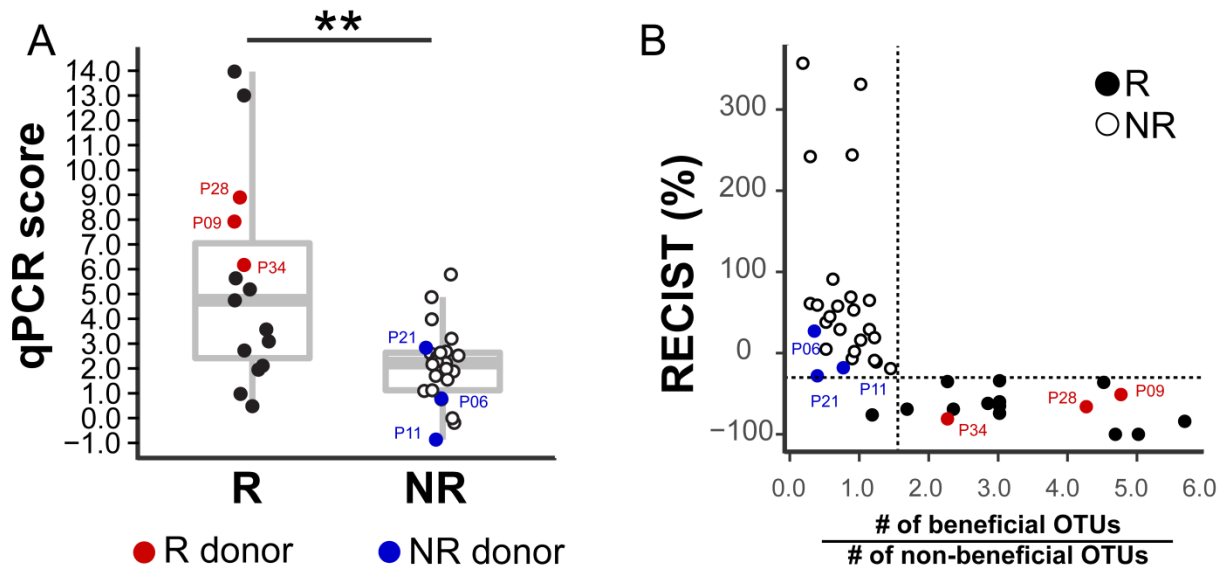


Fig. S7. Donor samples used in mouse colonization experiments are representative of the responder and non-responder patient groups with respect to qPCR score (**A**) and ratio of beneficial to non-beneficial OTUs (**B**) as in Figure 2. Wilcoxon-Mann-Whitney test (non-parametric) was used to compare qPCR score between R and NR groups same as in Figure 2D.

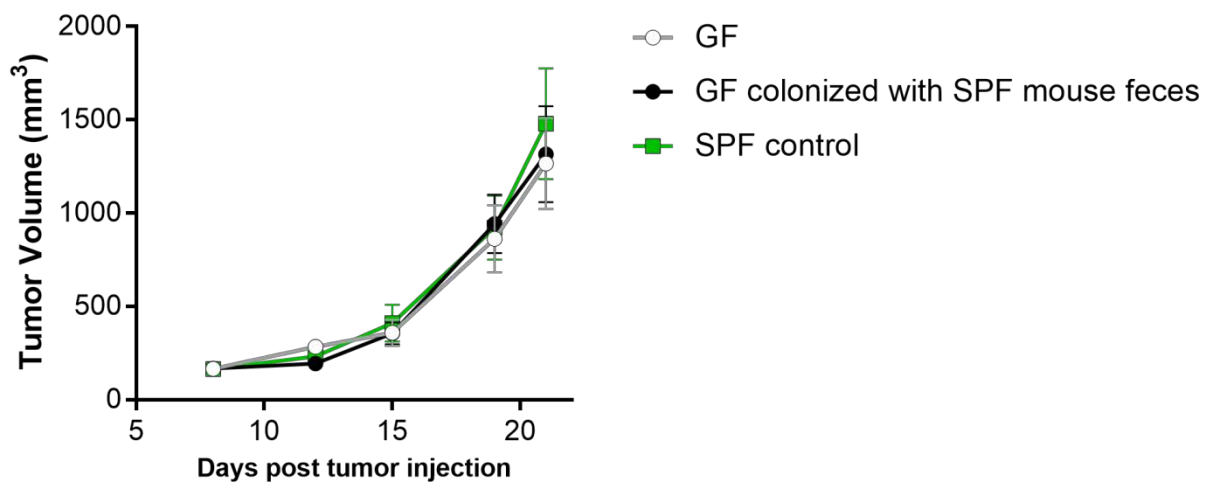


Fig. S8. Germ-free mice and Taconic SPF mice show similar tumor growth rates. Standard specific pathogen-free (SPF) mice were purchased from Taconic. Germ-free (GF) mice, originally purchased from Taconic were bred in the University of Chicago gnotobiotic facility. The GF mice were divided into two groups, and housed in two separate isolators in the same room. One group (black line; n=11) was colonized by oral gavage with fecal material from the SPF mice. The other group remained GF (grey line; n=10). Standard Taconic SPF mice (green line; n=5) were housed in ventilated cages in a standard barrier facility. All mice were maintained on the same diet. Two weeks later, the mice were injected with B16.SIY melanoma and tumor growth was measured.

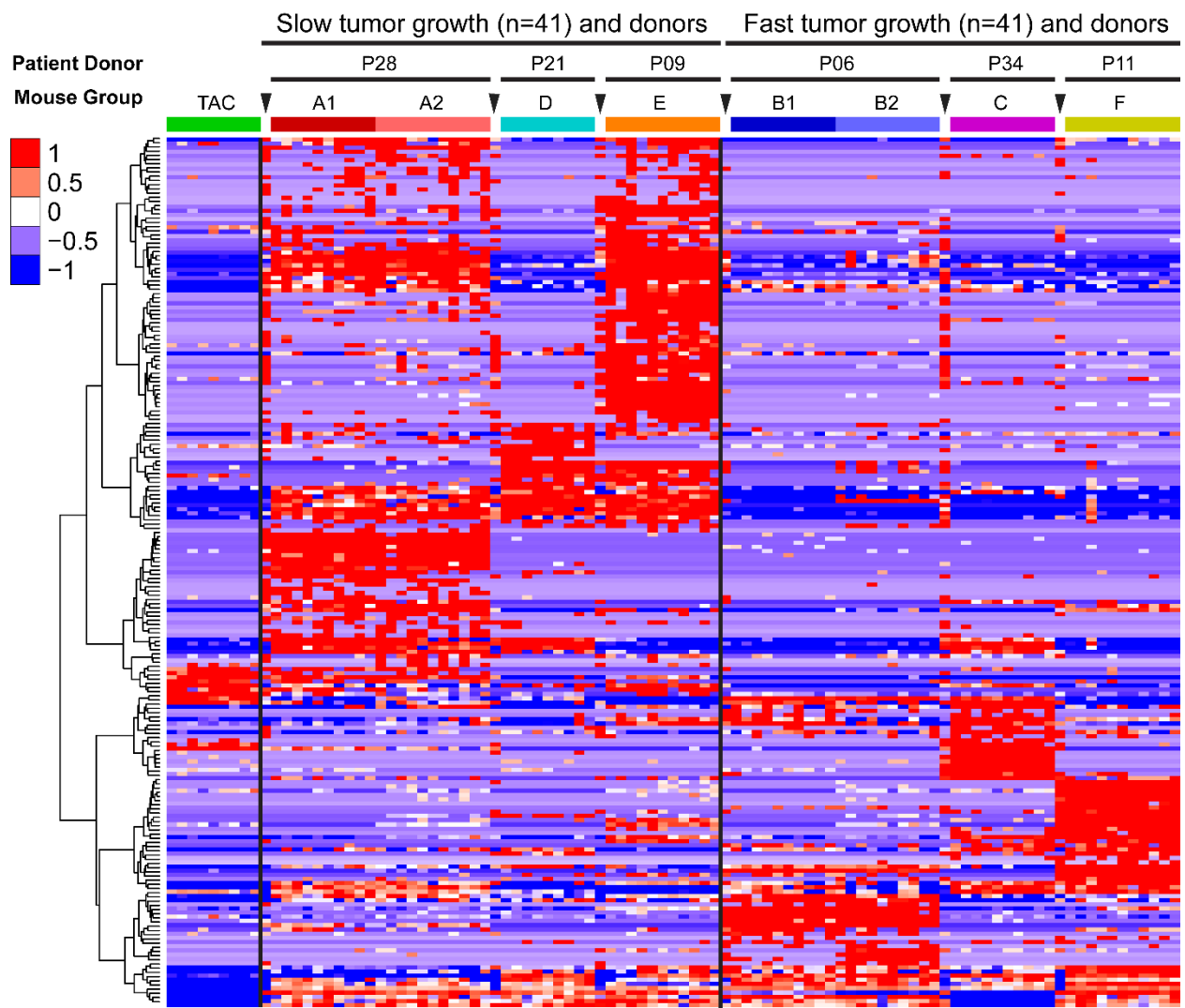


Fig. S9. Relative abundance of 207 OTUs from patient donors that colonized in mice, and were differentially abundant between slow and fast tumor growth groups. Columns depict individual mice arranged in groups A through F, with donor patient sample column indicated by arrow head, and donor ID shown above each mouse group. Rows indicate individual OTUs with exact reference ID match between human and mouse 16S rRNA data sets.

References and Notes

1. P. C. Tumeh, C. L. Harview, J. H. Yearley, I. P. Shintaku, E. J. Taylor, L. Robert, B. Chmielowski, M. Spasic, G. Henry, V. Ciobanu, A. N. West, M. Carmona, C. Kivork, E. Seja, G. Cherry, A. J. Gutierrez, T. R. Grogan, C. Mateus, G. Tomasic, J. A. Glaspy, R. O. Emerson, H. Robins, R. H. Pierce, D. A. Elashoff, C. Robert, A. Ribas, PD-1 blockade induces responses by inhibiting adaptive immune resistance. *Nature* **515**, 568–571 (2014). [doi:10.1038/nature13954](https://doi.org/10.1038/nature13954) [Medline](#)
2. M. Ayers, J. Lunceford, M. Nebozhyn, E. Murphy, A. Loboda, D. R. Kaufman, A. Albright, J. D. Cheng, S. P. Kang, V. Shankaran, S. A. Piha-Paul, J. Yearley, T. Y. Seiwert, A. Ribas, T. K. McClanahan, IFN- γ -related mRNA profile predicts clinical response to PD-1 blockade. *J. Clin. Invest.* **127**, 2930–2940 (2017). [doi:10.1172/JCI91190](https://doi.org/10.1172/JCI91190) [Medline](#)
3. L. Corrales, V. Matson, B. Flood, S. Spranger, T. F. Gajewski, Innate immune signaling and regulation in cancer immunotherapy. *Cell Res.* **27**, 96–108 (2017). [doi:10.1038/cr.2016.149](https://doi.org/10.1038/cr.2016.149) [Medline](#)
4. A. Sivan, L. Corrales, N. Hubert, J. B. Williams, K. Aquino-Michaels, Z. M. Earley, F. W. Benyamin, Y. M. Lei, B. Jabri, M. L. Alegre, E. B. Chang, T. F. Gajewski, Commensal *Bifidobacterium* promotes antitumor immunity and facilitates anti-PD-L1 efficacy. *Science* **350**, 1084–1089 (2015). [doi:10.1126/science.aac4255](https://doi.org/10.1126/science.aac4255) [Medline](#)
5. S. L. Topalian, F. S. Hodi, J. R. Brahmer, S. N. Gettinger, D. C. Smith, D. F. McDermott, J. D. Powderly, R. D. Carvajal, J. A. Sosman, M. B. Atkins, P. D. Leming, D. R. Spigel, S. J. Antonia, L. Horn, C. G. Drake, D. M. Pardoll, L. Chen, W. H. Sharfman, R. A. Anders, J. M. Taube, T. L. McMiller, H. Xu, A. J. Korman, M. Jure-Kunkel, S. Agrawal, D. McDonald, G. D. Kollia, A. Gupta, J. M. Wigginton, M. Sznol, Safety, activity, and immune correlates of anti-PD-1 antibody in cancer. *N. Engl. J. Med.* **366**, 2443–2454 (2012). [doi:10.1056/NEJMoa1200690](https://doi.org/10.1056/NEJMoa1200690) [Medline](#)
6. C. Robert, J. Schachter, G. V. Long, A. Arance, J. J. Grob, L. Mortier, A. Daud, M. S. Carlino, C. McNeil, M. Lotem, J. Larkin, P. Lorigan, B. Neyns, C. U. Blank, O. Hamid, C. Mateus, R. Shapira-Frommer, M. Kosh, H. Zhou, N. Ibrahim, S. Ebbinghaus, A. Ribas, KEYNOTE-006 investigators, Pembrolizumab versus ipilimumab in advanced melanoma. *N. Engl. J. Med.* **372**, 2521–2532 (2015). [doi:10.1056/NEJMoa1503093](https://doi.org/10.1056/NEJMoa1503093) [Medline](#)
7. B. Routy, E. Le Chatelier, L. Derosa, C. P. M. Duong, M. T. Alou, R. Daillière, A. Fluckiger, M. Messaoudene, C. Rauber, M. P. Roberti, M. Fidelle, C. Flament, V. Poirier-Colame, P. Opolon, C. Klein, K. Iribarren, L. Mondragón, N. Jacquemet, B. Qu, G. Ferrere, C. Clémenson, L. Mezquita, J. R. Masip, C. Naltet, S. Brosseau, C. Kaderbhai, C. Richard, H. Rizvi, F. Levenez, N. Galleron, B. Quinquis, N. Pons, B. Ryffel, V. Minard-Colin, P. Gonin, J. C. Soria, E. Deutsch, Y. Loriot, F. Ghiringhelli, G. Zalcman, F. Goldwasser, B. Escudier, M. D. Hellmann, A. Eggermont, D. Raoult, L. Albiges, G. Kroemer, L. Zitvogel, Gut microbiome influences efficacy of PD-1-based immunotherapy against epithelial tumors. *Science* **359**, 91 (2017). [Medline](#)
8. R. Daillière, M. Vétizou, N. Waldschmitt, T. Yamazaki, C. Isnard, V. Poirier-Colame, C. P. M. Duong, C. Flament, P. Lepage, M. P. Roberti, B. Routy, N. Jacquemet, L. Apetoh, S. Becharef, S. Rusakiewicz, P. Langella, H. Sokol, G. Kroemer, D. Enot, A. Roux, A.

- Eggermont, E. Tartour, L. Johannes, P. L. Woerther, E. Chachaty, J. C. Soria, E. Golden, S. Formenti, M. Plebanski, M. Madondo, P. Rosenstiel, D. Raoult, V. Cattoir, I. G. Boneca, M. Chamaillard, L. Zitvogel, *Enterococcus hirae* and *Barnesiella intestinihominis* facilitate cyclophosphamide-induced therapeutic immunomodulatory effects. *Immunity* **45**, 931–943 (2016). [doi:10.1016/j.immuni.2016.09.009](https://doi.org/10.1016/j.immuni.2016.09.009) Medline
9. N. Iida, A. Dzutsev, C. A. Stewart, L. Smith, N. Bouladoux, R. A. Weingarten, D. A. Molina, R. Salcedo, T. Back, S. Cramer, R. M. Dai, H. Kiu, M. Cardone, S. Naik, A. K. Patri, E. Wang, F. M. Marincola, K. M. Frank, Y. Belkaid, G. Trinchieri, R. S. Goldszmid, Commensal bacteria control cancer response to therapy by modulating the tumor microenvironment. *Science* **342**, 967–970 (2013). [doi:10.1126/science.1240527](https://doi.org/10.1126/science.1240527) Medline
10. M. Vétizou, J. M. Pitt, R. Daillère, P. Lepage, N. Waldschmitt, C. Flament, S. Rusakiewicz, B. Routy, M. P. Roberti, C. P. Duong, V. Poirier-Colame, A. Roux, S. Becharef, S. Formenti, E. Golden, S. Cording, G. Eberl, A. Schlitzer, F. Ginhoux, S. Mani, T. Yamazaki, N. Jacquemet, D. P. Enot, M. Bérard, J. Nigou, P. Opolon, A. Eggermont, P. L. Woerther, E. Chachaty, N. Chaput, C. Robert, C. Mateus, G. Kroemer, D. Raoult, I. G. Boneca, F. Carbonnel, M. Chamaillard, L. Zitvogel, Anticancer immunotherapy by CTLA-4 blockade relies on the gut microbiota. *Science* **350**, 1079–1084 (2015). [doi:10.1126/science.aad1329](https://doi.org/10.1126/science.aad1329) Medline
11. K. Atarashi, T. Tanoue, T. Shima, A. Imaoka, T. Kuwahara, Y. Momose, G. Cheng, S. Yamasaki, T. Saito, Y. Ohba, T. Taniguchi, K. Takeda, S. Hori, I. I. Ivanov II, Y. Umesaki, K. Itoh, K. Honda, Induction of colonic regulatory T cells by indigenous *Clostridium* species. *Science* **331**, 337–341 (2011). [doi:10.1126/science.1198469](https://doi.org/10.1126/science.1198469) Medline
12. J. L. Round, S. K. Mazmanian, Inducible Foxp³⁺ regulatory T-cell development by a commensal bacterium of the intestinal microbiota. *Proc. Natl. Acad. Sci. U.S.A.* **107**, 12204–12209 (2010). [doi:10.1073/pnas.0909122107](https://doi.org/10.1073/pnas.0909122107) Medline
13. N. Geva-Zatorsky, E. Sefik, L. Kua, L. Pasman, T. G. Tan, A. Ortiz-Lopez, T. B. Yanortsang, L. Yang, R. Jupp, D. Mathis, C. Benoist, D. L. Kasper, Mining the human gut microbiota for immunomodulatory organisms. *Cell* **168**, 928–943.e11 (2017). [doi:10.1016/j.cell.2017.01.022](https://doi.org/10.1016/j.cell.2017.01.022) Medline
14. V. Gopalakrishnan, C. N. Spencer, L. Nezi, A. Reuben, M. C. Andrews, T. V. Karpinets, P. A. Prieto, D. Vicente, K. Hoffman, S. C. Wei, A. P. Cogdill, L. Zhao, C. W. Hudgens, D. S. Hutchinson, T. Manzo, M. Petaccia de Macedo, T. Cotechini, T. Kumar, W. S. Chen, S. M. Reddy, R. S. Sloane, J. Galloway-Pena, H. Jiang, P. L. Chen, E. J. Shpall, K. Rezvani, A. M. Alousi, R. F. Chemaly, S. Shelburne, L. M. Vence, P. C. Okhuysen, V. B. Jensen, A. G. Swennes, F. McAllister, E. M. R. Sanchez, Y. Zhang, E. Le Chatelier, L. Zitvogel, N. Pons, J. L. Austin-Breneman, L. E. Haydu, E. M. Burton, J. M. Gardner, E. Sirmans, J. Hu, A. J. Lazar, T. Tsujikawa, A. Diab, H. Tawbi, I. C. Glitza, W. J. Hwu, S. P. Patel, S. E. Woodman, R. N. Amaria, M. A. Davies, J. E. Gershenwald, P. Hwu, J. E. Lee, J. Zhang, L. M. Coussens, Z. A. Cooper, P. A. Futreal, C. R. Daniel, N. J. Ajami, J. F. Petrosino, M. T. Tetzlaff, P. Sharma, J. P. Allison, R. R. Jenq, J. A. Wargo, Gut microbiome modulates response to anti-PD-1 immunotherapy in melanoma patients. *Science* eaan4236 (2017). [doi:10.1126/science.eaan4236](https://doi.org/10.1126/science.eaan4236) Medline

15. S. Spranger, R. Bao, T. F. Gajewski, Melanoma-intrinsic β -catenin signalling prevents anti-tumour immunity. *Nature* **523**, 231–235 (2015). [doi:10.1038/nature14404](https://doi.org/10.1038/nature14404) [Medline](#)
16. W. Peng, J. Q. Chen, C. Liu, S. Malu, C. Creasy, M. T. Tetzlaff, C. Xu, J. A. McKenzie, C. Zhang, X. Liang, L. J. Williams, W. Deng, G. Chen, R. Mbafung, A. J. Lazar, C. A. Torres-Cabala, Z. A. Cooper, P. L. Chen, T. N. Tieu, S. Spranger, X. Yu, C. Bernatchez, M. A. Forget, C. Haymaker, R. Amaria, J. L. McQuade, I. C. Glitza, T. Cascone, H. S. Li, L. N. Kwong, T. P. Heffernan, J. Hu, R. L. Bassett Jr., M. W. Bosenberg, S. E. Woodman, W. W. Overwijk, G. Lizée, J. Roszik, T. F. Gajewski, J. A. Wargo, J. E. Gershenwald, L. Radvanyi, M. A. Davies, P. Hwu, Loss of PTEN promotes resistance to T cell-mediated immunotherapy. *Cancer Discov.* **6**, 202–216 (2016). [doi:10.1158/2159-8290.CD-15-0283](https://doi.org/10.1158/2159-8290.CD-15-0283) [Medline](#)
17. S. Uigurel, D. Schrama, G. Keller, D. Schadendorf, E. B. Bröcker, R. Houben, M. Zapata, W. Fink, H. L. Kaufman, J. C. Becker, Impact of the CCR5 gene polymorphism on the survival of metastatic melanoma patients receiving immunotherapy. *Cancer Immunol. Immunother.* **57**, 685–691 (2008). [doi:10.1007/s00262-007-0407-z](https://doi.org/10.1007/s00262-007-0407-z) [Medline](#)
18. J. G. Caporaso, C. L. Lauber, W. A. Walters, D. Berg-Lyons, J. Huntley, N. Fierer, S. M. Owens, J. Betley, L. Fraser, M. Bauer, N. Gormley, J. A. Gilbert, G. Smith, R. Knight, Ultra-high-throughput microbial community analysis on the Illumina HiSeq and MiSeq platforms. *ISME J.* **6**, 1621–1624 (2012). [doi:10.1038/ismej.2012.8](https://doi.org/10.1038/ismej.2012.8) [Medline](#)
19. J. G. Caporaso, C. L. Lauber, W. A. Walters, D. Berg-Lyons, C. A. Lozupone, P. J. Turnbaugh, N. Fierer, R. Knight, Global patterns of 16S rRNA diversity at a depth of millions of sequences per sample. *Proc. Natl. Acad. Sci. U.S.A.* **108** (Suppl 1), 4516–4522 (2011). [doi:10.1073/pnas.1000080107](https://doi.org/10.1073/pnas.1000080107) [Medline](#)
20. J. G. Caporaso, J. Kuczynski, J. Stombaugh, K. Bittinger, F. D. Bushman, E. K. Costello, N. Fierer, A. G. Peña, J. K. Goodrich, J. I. Gordon, G. A. Hutley, S. T. Kelley, D. Knights, J. E. Koenig, R. E. Ley, C. A. Lozupone, D. McDonald, B. D. Muegge, M. Pirrung, J. Reeder, J. R. Sevinsky, P. J. Turnbaugh, W. A. Walters, J. Widmann, T. Yatsunenko, J. Zaneveld, R. Knight, QIIME allows analysis of high-throughput community sequencing data. *Nat. Methods* **7**, 335–336 (2010). [doi:10.1038/nmeth.f.303](https://doi.org/10.1038/nmeth.f.303) [Medline](#)
21. D. McDonald, M. N. Price, J. Goodrich, E. P. Nawrocki, T. Z. DeSantis, A. Probst, G. L. Andersen, R. Knight, P. Hugenholtz, An improved Greengenes taxonomy with explicit ranks for ecological and evolutionary analyses of bacteria and archaea. *ISME J.* **6**, 610–618 (2012). [doi:10.1038/ismej.2011.139](https://doi.org/10.1038/ismej.2011.139) [Medline](#)
22. J. G. Caporaso, K. Bittinger, F. D. Bushman, T. Z. DeSantis, G. L. Andersen, R. Knight, PyNAST: A flexible tool for aligning sequences to a template alignment. *Bioinformatics* **26**, 266–267 (2010). [doi:10.1093/bioinformatics/btp636](https://doi.org/10.1093/bioinformatics/btp636) [Medline](#)
23. R. C. Edgar, Search and clustering orders of magnitude faster than BLAST. *Bioinformatics* **26**, 2460–2461 (2010). [doi:10.1093/bioinformatics/btq461](https://doi.org/10.1093/bioinformatics/btq461) [Medline](#)
24. N. Segata, L. Waldron, A. Ballarini, V. Narasimhan, O. Jousson, C. Huttenhower, Metagenomic microbial community profiling using unique clade-specific marker genes. *Nat. Methods* **9**, 811–814 (2012). [doi:10.1038/nmeth.2066](https://doi.org/10.1038/nmeth.2066) [Medline](#)

25. B. A. Methé, K. E. Nelson, M. Pop, H. H. Creasy, M. G. Giglio, C. Huttenhower, D. Gevers, J. F. Petrosino, S. Abubucker, J. H. Badger, A. T. Chinwalla, A. M. Earl, M. G. FitzGerald, R. S. Fulton, K. Hallsworth-Pepin, E. A. Lobos, R. Madupu, V. Magrini, J. C. Martin, M. Mitreva, D. M. Muzny, E. J. Sodergren, J. Versalovic, A. M. Wollam, K. C. Worley, J. R. Wortman, S. K. Young, Q. Zeng, K. M. Aagaard, O. O. Abolude, E. Allen-Vercoe, E. J. Alm, L. Alvarado, G. L. Andersen, S. Anderson, E. Appelbaum, H. M. Arachchi, G. Armitage, C. A. Arze, T. Ayvaz, C. C. Baker, L. Begg, T. Belachew, V. Bhonagiri, M. Bihan, M. J. Blaser, T. Bloom, V. R. Bonazzi, P. Brooks, G. A. Buck, C. J. Buhay, D. A. Busam, J. L. Campbell, S. R. Canon, B. L. Cantarel, P. S. Chain, I.-M. A. Chen, L. Chen, S. Chhibba, K. Chu, D. M. Ciulla, J. C. Clemente, S. W. Clifton, S. Conlan, J. Crabtree, M. A. Cutting, N. J. Davidovics, C. C. Davis, T. Z. DeSantis, C. Deal, K. D. Delehaunty, F. E. Dewhirst, E. Deych, Y. Ding, D. J. Dooling, S. P. Dugan, W. Michael Dunne, A. Scott Durkin, R. C. Edgar, R. L. Erlich, C. N. Farmer, R. M. Farrell, K. Faust, M. Feldgarden, V. M. Felix, S. Fisher, A. A. Fodor, L. Forney, L. Foster, V. Di Francesco, J. Friedman, D. C. Friedrich, C. C. Fronick, L. L. Fulton, H. Gao, N. Garcia, G. Giannoukos, C. Giblin, M. Y. Giovanni, J. M. Goldberg, J. Goll, A. Gonzalez, A. Griggs, S. Gujja, B. J. Haas, H. A. Hamilton, E. L. Harris, T. A. Hepburn, B. Herter, D. E. Hoffmann, M. E. Holder, C. Howarth, K. H. Huang, S. M. Huse, J. Izard, J. K. Jansson, H. Jiang, C. Jordan, V. Joshi, J. A. Katancik, W. A. Keitel, S. T. Kelley, C. Kells, S. Kinder-Haake, N. B. King, R. Knight, D. Knights, H. H. Kong, O. Koren, S. Koren, K. C. Kota, C. L. Kovar, N. C. Kyrpides, P. S. La Rosa, S. L. Lee, K. P. Lemon, N. Lennon, C. M. Lewis, L. Lewis, R. E. Ley, K. Li, K. Liolios, B. Liu, Y. Liu, C.-C. Lo, C. A. Lozupone, R. Dwayne Lunsford, T. Madden, A. A. Mahurkar, P. J. Mannon, E. R. Mardis, V. M. Markowitz, K. Mavrommatis, J. M. McCorrison, D. McDonald, J. McEwen, A. L. McGuire, P. McInnes, T. Mehta, K. A. Mihindukulasuriya, J. R. Miller, P. J. Minx, I. Newsham, C. Nusbaum, M. O'Laughlin, J. Orvis, I. Pagani, K. Palaniappan, S. M. Patel, M. Pearson, J. Peterson, M. Podar, C. Pohl, K. S. Pollard, M. E. Priest, L. M. Proctor, X. Qin, J. Raes, J. Ravel, J. G. Reid, M. Rho, R. Rhodes, K. P. Riehle, M. C. Rivera, B. Rodriguez-Mueller, Y.-H. Rogers, M. C. Ross, C. Russ, R. K. Sanka, P. Sankar, J. Fah Sathirapongsasuti, J. A. Schloss, P. D. Schloss, T. M. Schmidt, M. Scholz, L. Schriml, A. M. Schubert, N. Segata, J. A. Segre, W. D. Shannon, R. R. Sharp, T. J. Sharpton, N. Shenoy, N. U. Sheth, G. A. Simone, I. Singh, C. S. Smillie, J. D. Sobel, D. D. Sommer, P. Spicer, G. G. Sutton, S. M. Sykes, D. G. Tabbaa, M. Thiagarajan, C. M. Tomlinson, M. Torralba, T. J. Treangen, R. M. Truty, T. A. Vishnivetskaya, J. Walker, L. Wang, Z. Wang, D. V. Ward, W. Warren, M. A. Watson, C. Wellington, K. A. Wetterstrand, J. R. White, K. Wilczek-Boney, Y. Qing Wu, K. M. Wylie, T. Wylie, C. Yandava, L. Ye, Y. Ye, S. Yoosoph, B. P. Youmans, L. Zhang, Y. Zhou, Y. Zhu, L. Zoloth, J. D. Zucker, B. W. Birren, R. A. Gibbs, S. K. Highlander, G. M. Weinstock, R. K. Wilson, O. White, Human Microbiome Project Consortium, A framework for human microbiome research. *Nature* **486**, 215–221 (2012).

[doi:10.1038/nature11209](https://doi.org/10.1038/nature11209) [Medline](#)

26. M. C. Collado, M. Derrien, E. Isolauri, W. M. de Vos, S. Salminen, Intestinal integrity and *Akkermansia muciniphila*, a mucin-degrading member of the intestinal microbiota present in infants, adults, and the elderly. *Appl. Environ. Microbiol.* **73**, 7767–7770 (2007).

[doi:10.1128/AEM.01477-07](https://doi.org/10.1128/AEM.01477-07) [Medline](#)

27. J. Junick, M. Blaut, Quantification of human fecal bifidobacterium species by use of quantitative real-time PCR analysis targeting the groEL gene. *Appl. Environ. Microbiol.* **78**, 2613–2622 (2012). [doi:10.1128/AEM.07749-11](https://doi.org/10.1128/AEM.07749-11) [Medline](#)
28. E. Malinen, A. Kassinen, T. Rinttilä, A. Palva, Comparison of real-time PCR with SYBR Green I or 5'-nuclease assays and dot-blot hybridization with rDNA-targeted oligonucleotide probes in quantification of selected faecal bacteria. *Microbiology* **149**, 269–277 (2003). [doi:10.1099/mic.0.25975-0](https://doi.org/10.1099/mic.0.25975-0) [Medline](#)
29. T. Matsuki, K. Watanabe, R. Tanaka, H. Oyaizu, Rapid identification of human intestinal *Bifidobacteria* by 16S rRNA-targeted species- and group-specific primers. *FEMS Microbiol. Lett.* **167**, 113–121 (1998). [doi:10.1111/j.1574-6968.1998.tb13216.x](https://doi.org/10.1111/j.1574-6968.1998.tb13216.x) [Medline](#)
30. A. Kassinen, L. Krogius-Kurikka, H. Mäkivuokko, T. Rinttilä, L. Paulin, J. Corander, E. Malinen, J. Apajalahti, A. Palva, The fecal microbiota of irritable bowel syndrome patients differs significantly from that of healthy subjects. *Gastroenterology* **133**, 24–33 (2007). [doi:10.1053/j.gastro.2007.04.005](https://doi.org/10.1053/j.gastro.2007.04.005) [Medline](#)
31. I. U. Rathnayake, M. Hargreaves, F. Huygens, Genotyping of *Enterococcus faecalis* and *Enterococcus faecium* isolates by use of a set of eight single nucleotide polymorphisms. *J. Clin. Microbiol.* **49**, 367–372 (2011). [doi:10.1128/JCM.01120-10](https://doi.org/10.1128/JCM.01120-10) [Medline](#)
32. T. Rinttilä, A. Kassinen, E. Malinen, L. Krogius, A. Palva, Development of an extensive set of 16S rDNA-targeted primers for quantification of pathogenic and indigenous bacteria in faecal samples by real-time PCR. *J. Appl. Microbiol.* **97**, 1166–1177 (2004). [doi:10.1111/j.1365-2672.2004.02409.x](https://doi.org/10.1111/j.1365-2672.2004.02409.x) [Medline](#)
33. Z. Sun, Z. Chen, X. Hou, S. Li, H. Zhu, J. Qian, D. Lu, W. Liu, Locked nucleic acid pentamers as universal PCR primers for genomic DNA amplification. *PLOS ONE* **3**, e3701 (2008). [doi:10.1371/journal.pone.0003701](https://doi.org/10.1371/journal.pone.0003701) [Medline](#)
34. K. Matsuda, H. Tsuji, T. Asahara, K. Matsumoto, T. Takada, K. Nomoto, Establishment of an analytical system for the human fecal microbiota, based on reverse transcription-quantitative PCR targeting of multicopy rRNA molecules. *Appl. Environ. Microbiol.* **75**, 1961–1969 (2009). [doi:10.1128/AEM.01843-08](https://doi.org/10.1128/AEM.01843-08) [Medline](#)
35. P. Louis, S. I. McCrae, C. Charrier, H. J. Flint, Organization of butyrate synthetic genes in human colonic bacteria: Phylogenetic conservation and horizontal gene transfer. *FEMS Microbiol. Lett.* **269**, 240–247 (2007). [doi:10.1111/j.1574-6968.2006.00629.x](https://doi.org/10.1111/j.1574-6968.2006.00629.x) [Medline](#)
36. X. W. Huijsdens, R. K. Linskens, M. Mak, S. G. Meuwissen, C. M. Vandebroucke-Grauls, P. H. Savelkoul, Quantification of bacteria adherent to gastrointestinal mucosa by real-time PCR. *J. Clin. Microbiol.* **40**, 4423–4427 (2002). [doi:10.1128/JCM.40.12.4423-4427.2002](https://doi.org/10.1128/JCM.40.12.4423-4427.2002) [Medline](#)
37. J. Tong, C. Liu, P. Summanen, H. Xu, S. M. Finegold, Application of quantitative real-time PCR for rapid identification of *Bacteroides fragilis* group and related organisms in human wound samples. *Anaerobe* **17**, 64–68 (2011). [doi:10.1016/j.anaerobe.2011.03.004](https://doi.org/10.1016/j.anaerobe.2011.03.004) [Medline](#)
38. H. Yampara-Iquise, G. Zheng, J. E. Jones, C. A. Carson, Use of a *Bacteroides* thetaiotaomicron-specific α-1-6, mannanase quantitative PCR to detect human faecal

- pollution in water. *J. Appl. Microbiol.* **105**, 1686–1693 (2008). [doi:10.1111/j.1365-2672.2008.03895.x](https://doi.org/10.1111/j.1365-2672.2008.03895.x) [Medline](#)
39. S. J. Song, C. Lauber, E. K. Costello, C. A. Lozupone, G. Humphrey, D. Berg-Lyons, J. G. Caporaso, D. Knights, J. C. Clemente, S. Nakielny, J. I. Gordon, N. Fierer, R. Knight, Cohabiting family members share microbiota with one another and with their dogs. *eLife* **2**, e00458 (2013). [doi:10.7554/eLife.00458](https://doi.org/10.7554/eLife.00458) [Medline](#)
40. C. G. Buffie, I. Jarchum, M. Equinda, L. Lipuma, A. Gobourne, A. Viale, C. Ubeda, J. Xavier, E. G. Pamer, Profound alterations of intestinal microbiota following a single dose of clindamycin results in sustained susceptibility to *Clostridium difficile*-induced colitis. *Infect. Immun.* **80**, 62–73 (2012). [doi:10.1128/IAI.05496-11](https://doi.org/10.1128/IAI.05496-11) [Medline](#)
41. S. Andrews, Q. C. Fast, A quality control application for high throughput sequence data (Babraham Institute, 2016); www.bioinformatics.babraham.ac.uk/projects/fastqc.
42. N. L. Bray, H. Pimentel, P. Melsted, L. Pachter, Near-optimal probabilistic RNA-seq quantification. *Nat. Biotechnol.* **34**, 525–527 (2016). [doi:10.1038/nbt.3519](https://doi.org/10.1038/nbt.3519) [Medline](#)
43. C. Soneson, M. I. Love, M. D. Robinson, Differential analyses for RNA-seq: Transcript-level estimates improve gene-level inferences. *F1000Res.* **4**, 1521 (2015). [doi:10.12688/f1000research.7563.1](https://doi.org/10.12688/f1000research.7563.1) [Medline](#)
44. H. Li, Aligning sequence reads, clone sequences and assembly contigs with BWA-MEM. [arXiv:1303.3997v2](https://arxiv.org/abs/1303.3997v2) [q-bio.GN] (26 May 2013).
45. A. Tarasov, A. J. Vilella, E. Cuppen, I. J. Nijman, P. Prins, Sambamba: Fast processing of NGS alignment formats. *Bioinformatics* **31**, 2032–2034 (2015). [doi:10.1093/bioinformatics/btv098](https://doi.org/10.1093/bioinformatics/btv098) [Medline](#)
46. G. A. Van der Auwera, M. O. Carneiro, C. Hartl, R. Poplin, G. Del Angel, A. Levy-Moonshine, T. Jordan, K. Shakir, D. Roazen, J. Thibault, E. Banks, K. V. Garimella, D. Altshuler, S. Gabriel, M. A. DePristo, From FastQ data to high confidence variant calls: The Genome Analysis Toolkit best practices pipeline. *Curr. Protoc. Bioinformatics* **43**, 1–33 (2013). [Medline](#)
47. K. Cibulskis, M. S. Lawrence, S. L. Carter, A. Sivachenko, D. Jaffe, C. Sougnez, S. Gabriel, M. Meyerson, E. S. Lander, G. Getz, Sensitive detection of somatic point mutations in impure and heterogeneous cancer samples. *Nat. Biotechnol.* **31**, 213–219 (2013). [doi:10.1038/nbt.2514](https://doi.org/10.1038/nbt.2514) [Medline](#)
48. A. Auton, L. D. Brooks, R. M. Durbin, E. P. Garrison, H. M. Kang, J. O. Korbel, J. L. Marchini, S. McCarthy, G. A. McVean, G. R. Abecasis; 1000 Genomes Project Consortium, A global reference for human genetic variation. *Nature* **526**, 68–74 (2015). [Medline](#)
49. W. Fu, T. D. O'Connor, G. Jun, H. M. Kang, G. Abecasis, S. M. Leal, S. Gabriel, M. J. Rieder, D. Altshuler, J. Shendure, D. A. Nickerson, M. J. Bamshad, J. M. Akey, NHLBI Exome Sequencing Project, Analysis of 6,515 exomes reveals the recent origin of most human protein-coding variants. *Nature* **493**, 216–220 (2013). [doi:10.1038/nature11690](https://doi.org/10.1038/nature11690) [Medline](#)

50. M. Lek, K. J. Karczewski, E. V. Minikel, K. E. Samocha, E. Banks, T. Fennell, A. H. O'Donnell-Luria, J. S. Ware, A. J. Hill, B. B. Cummings, T. Tukiainen, D. P. Birnbaum, J. A. Kosmicki, L. E. Duncan, K. Estrada, F. Zhao, J. Zou, E. Pierce-Hoffman, J. Berghout, D. N. Cooper, N. Deflaux, M. DePristo, R. Do, J. Flannick, M. Fromer, L. Gauthier, J. Goldstein, N. Gupta, D. Howrigan, A. Kiezun, M. I. Kurki, A. L. Moonshine, P. Natarajan, L. Orozco, G. M. Peloso, R. Poplin, M. A. Rivas, V. Ruano-Rubio, S. A. Rose, D. M. Ruderfer, K. Shakir, P. D. Stenson, C. Stevens, B. P. Thomas, G. Tiao, M. T. Tusie-Luna, B. Weisburd, H. H. Won, D. M. Altshuler, D. Ardiissino, M. Boehnke, J. Danesh, S. Donnelly, R. Elosua, J. C. Florez, S. B. Gabriel, G. Getz, S. J. Glatt, C. M. Hultman, S. Kathiresan, M. Laakso, S. McCarroll, M. I. McCarthy, D. McGovern, R. McPherson, B. M. Neale, A. Palotie, S. M. Purcell, D. Saleheen, J. M. Scharf, P. Sklar, P. F. Sullivan, J. Tuomilehto, M. T. Tsuang, H. C. Watkins, J. G. Wilson, M. J. Daly, D. G. MacArthur, Exome Aggregation Consortium, Analysis of protein-coding genetic variation in 60,706 humans. *Nature* **536**, 285–291 (2016).
[doi:10.1038/nature19057](https://doi.org/10.1038/nature19057) [Medline](#)
51. K. Wang, M. Li, H. Hakonarson, ANNOVAR: Functional annotation of genetic variants from high-throughput sequencing data. *Nucleic Acids Res.* **38**, e164 (2010).
[doi:10.1093/nar/gkq603](https://doi.org/10.1093/nar/gkq603) [Medline](#)
52. C. Blank, I. Brown, A. C. Peterson, M. Spiotto, Y. Iwai, T. Honjo, T. F. Gajewski, PD-L1/B7H-1 inhibits the effector phase of tumor rejection by T cell receptor (TCR) transgenic CD8+ T cells. *Cancer Res.* **64**, 1140–1145 (2004). [doi:10.1158/0008-5472.CAN-03-3259](https://doi.org/10.1158/0008-5472.CAN-03-3259) [Medline](#)
53. Y. Benjamini, Y. Hochberg, Controlling the false discovery rate—A practical and powerful approach to multiple testing. *J. R. Stat. Soc. Series B Stat. Methodol.* **57**, 289–300 (1995).